Communication

Radially Phased-Locked Hermite–Gaussian Correlated Beam Array and Its Properties in Oceanic Turbulence

Peiying Zhu, Guiqiu Wang *, Yan Yin, Haiyang Zhong, Yaochuan Wang and Dajun Liu *

Department of Physics, College of Science, Dalian Maritime University, Dalian 116026, China
* Correspondence: gqwang@dlmu.edu.cn (G.W.); liudajun@dlmu.edu.cn (D.L.)

Abstract: The descriptions of a radially phased-locked Hermite–Gaussian correlated beam array are introduced, the equation of this beam array in oceanic turbulence is derived, and the intensity profiles of this beam array are shown and analyzed. The results imply that the evolutions of the sub-beam of this beam array in free space are the same as the Hermite–Gaussian correlated beam, while the intensity of this beam array can be adjusted by controlling the initial beam radius R and the coherence length. The intensity profiles of this beam array in free space have multiple spots during propagation, while the same beam array in oceanic turbulence can become a beam spot due to the influences of R and oceanic turbulence. The beam array with smaller coherence length in oceanic turbulence retains the splitting properties better during propagation.

Keywords: beam array; correlation function; intensity; oceanic turbulence

1. Introduction

The characteristics of laser transmitting in underwater turbulence affect the performances of underwater optical communication [1], and the propagation of beams in underwater turbulence has recently been widely studied. Partially coherent beams (PCBs) reduce the degrading effects of turbulence [2], and the structured light can remain invariant during propagation [3]. Previously, the scintillation properties of waves in underwater turbulence have been analyzed [4–6]. To examine the performances of underwater optical systems, the BER properties of laser in oceanic turbulence were investigated [7,8]. PCBs with unique correlation functions have been introduced into the underwater turbulence environments. The propagation of a multi-sinc Schell-model beam in anisotropic oceanic turbulence has been investigated [9]. The self-splitting structured beam can lower the negative influences of oceanic turbulence, which is achieved by controlling the parameters of the beams [10]. The influences of oceanic turbulence on non-uniformly correlated beams have been studied by numerical simulation [11,12]. The propagation of vortex beams in oceanic turbulence has been investigated, and neural networks have also been used in studies of vortex beams in underwater turbulence [13–17]. The beam array has a lattice-like intensity, and the properties of the beam array have been widely analyzed [18,19].

The PCBs' shaping can be modulated by coherence structure engineering [20], and PCBs can be experimentally generated [21]. The cross-spectral density (CSD) of PCBs with different coherence function has been widely discussed. The multi-Gaussian Schell-model beam (multi-GSM) has a flat-topped intensity profile in the far field [22]. The Gaussian intensity array can be obtained by anisotropic GSM beam array [23]. The Laguerre-Gaussian correlated beam can obtain the ring-shaped intensity distribution for propagation in free space [24]. The Hermite–Gaussian correlated Schell-model (HGCSM) beam can split from one beam spot to multiple spots [25]. Non-uniform PCB modulated by a non-uniform HGCSM function has been described, with the position of maximum intensity adjusted using the beam parameters [26]. The twist HGCSM beam can be obtained by introducing the twist phase [27]. In practice, the beam array can achieve high power, and can be

composed of off-axis beams [28,29]. The radial intensity distribution of the beam array can be obtained by radially phase-locked PCBs [30–32]. The splitting properties of HGCSM are very interesting. However, the beam array composed of HGCSM sub-beams has not yet been reported. In this work, the HGSM beam was extended into beam array. The CSD of a radially phased-locked HGCSM (RPLHGSM) beam array is introduced based on the HGCSM beam, and the intensity distributions of this beam array transmitting in oceanic turbulence are numerically analyzed. The paper is organized as follows. In Section 2, the CSD of an RPLHGSM beam array on the source plane is introduced. In Section 3, the propagation equation of an RPLHGSM beam array in oceanic turbulence is derived. In Section 4, the intensity profiles of this beam array in oceanic turbulence are discussed.

2. Model of an RPLHGSM Beam Array

The CSD of the HGCSM beam on the source plane $z = 0$ in the space-frequency domain is written as [24]:

$$W(\mathbf{r}_1, \mathbf{r}_2, 0) = C_0 \exp\left(-\frac{\mathbf{r}_1^2 + \mathbf{r}_2^2}{4w_0^2}\right) \exp\left[-\frac{(x_2 - x_1)^2}{2\delta_{0x}^2}\right] \frac{H_{2m}\left[\frac{x_2 - x_1}{\sqrt{2}\delta_{0x}}\right]}{H_{2m}(0)}$$
$$\exp\left[-\frac{(y_2 - y_1)^2}{2\delta_{0y}^2}\right] \frac{H_{2n}\left[\frac{y_2 - y_1}{\sqrt{2}\delta_{0y}}\right]}{H_{2n}(0)} \tag{1}$$

In Equation (1), $\mathbf{r} = (x, y)$ is the position vector, C_0 is a constant, w_0 represents beam width of Gauss part, δ_{0x} and δ_{0y} denote coherence length along x and y directions, respectively. H_m is the Hermite polynomial of order m and can be given as [33]:

$$H_m(x) = \sum_{l=0}^{[m/2]} \frac{(-1)^l m!}{l!(m-2l)!} (2x)^{m-2l} \tag{2}$$

Recalling the descriptions of beam array [27,34–36], the center of sub-beam of a beam array is set as (r_x, r_y), the CSD of an RPLHGSM beam array composed of N HGCSM sub-beams with radial distributions at source plane $z = 0$ can be given as:

$$W(\mathbf{r}_1, \mathbf{r}_2, 0) = C_0 \sum_{h_1=1}^{N} \exp\left[-\frac{\left(x_1 - r_{h_1 x}\right)^2 + \left(y_1 - r_{h_1 y}\right)^2}{4w_0^2}\right]$$
$$\times \sum_{h_2=1}^{N} \exp\left[-\frac{\left(x_2 - r_{h_2 x}\right)^2 + \left(y_2 - r_{h_2 y}\right)^2}{4w_0^2}\right]$$
$$\times \exp\left[-\frac{\left[\left(x_1 - r_{h_1 x}\right) - \left(x_2 - r_{h_2 x}\right)\right]^2}{2\delta_{0x}^2}\right] \exp\left[-\frac{\left[\left(y_1 - r_{h_1 y}\right) - \left(y_2 - r_{h_2 y}\right)\right]^2}{2\delta_{0y}^2}\right] \tag{3}$$
$$\times \frac{H_{2m}\left[\frac{\left(x_2 - r_{h_2 x}\right) - \left(x_1 - r_{h_1 x}\right)}{\sqrt{2}\delta_{0x}}\right]}{H_{2m}(0)} \frac{H_{2n}\left[\frac{\left(y_2 - r_{h_2 y}\right) - \left(y_1 - r_{h_1 y}\right)}{\sqrt{2}\delta_{0y}}\right]}{H_{2n}(0)}$$
$$\times \exp\left[i\left(\varphi_{h_1} - \varphi_{h_2}\right)\right]$$

where N is the number of sub-beams, R is the radius, $r_{hx} = R\cos\varphi_h$, $r_{hy} = R\sin\varphi_h$, $\varphi_h = h2\pi/N$, $(h = 1, 2, \ldots N)$ is the phase of the h-th sub-beam.

3. Propagation of an RPLHGSM Beam Array in Oceanic Turbulence

The CSD of PCBs propagating in oceanic turbulence is described by the extended Huygens–Fresnel principle [9–19]:

$$
\begin{aligned}
W(\boldsymbol{\rho}_1, \boldsymbol{\rho}_2, z) = \frac{k^2}{4\pi^2 z^2} \int_{-\infty}^{+\infty} \int_{-\infty}^{+\infty} \int_{-\infty}^{+\infty} \int_{-\infty}^{+\infty} W(\mathbf{r}_1, \mathbf{r}_2, 0) \\
\times \exp\left[-\frac{ik}{2z}(\boldsymbol{\rho}_1 - \mathbf{r}_1)^2 + \frac{ik}{2z}(\boldsymbol{\rho}_2 - \mathbf{r}_2)^2 \right] \\
\times \langle \exp[\psi(\mathbf{r}_1, \boldsymbol{\rho}_1) + \psi^*(\mathbf{r}_2, \boldsymbol{\rho}_2)] \rangle d\mathbf{r}_1 d\mathbf{r}_2
\end{aligned}
\tag{4}
$$

with

$$
\langle \exp[\psi(\mathbf{r}_1, \boldsymbol{\rho}_1) + \psi^*(\mathbf{r}_2, \boldsymbol{\rho}_2)] \rangle = \exp\left[-\frac{(\mathbf{r}_1 - \mathbf{r}_2)^2 + (\mathbf{r}_1 - \mathbf{r}_2)\cdot(\boldsymbol{\rho}_1 - \boldsymbol{\rho}_2) + (\boldsymbol{\rho}_1 - \boldsymbol{\rho}_2)^2}{\Lambda_0^2} \right]
\tag{5}
$$

where $1/\Lambda_0^2 = \pi^2 k^2 z T_0/3$, and $T_0 = \int \kappa^3 \Phi(\kappa) d\kappa$. $\Phi(\kappa)$ is the power spectrum of oceanic turbulence and is given as [37]:

$$
\begin{aligned}
\Phi(\kappa) = 0.388 \times 10^{-8} \varepsilon^{-1/3} \kappa^{-11/3} \chi_T \left[1 + 2.35(\kappa\eta)^{2/3} \right] \\
\times \left[\exp(-A_T \Theta) + \varsigma^{-2} \exp(-A_S \Theta) - 2\varsigma^{-1} \exp(-A_{TS}\Theta) \right]
\end{aligned}
\tag{6}
$$

The κ is the spatial frequency of power spectrum of oceanic turbulence. η is the Kolmogorov micro scale. χ_T, ε and ς are parameters of oceanic turbulence [36]. The parameters in Equation (6) are $A_T = 1.863 \times 10^{-2}$, $A_S = 1.9 \times 10^{-4}$, $A_{TS} = 9.41 \times 10^{-3}$, $\Theta = 8.284(\kappa\eta)^{4/3} + 12.978(\kappa\eta)^2$. The T_0 can be given as [12]:

$$
T_0 = 0.388 \times 10^{-8}(\varepsilon\eta)^{-1/3}\left(47.5708\varsigma^{-2} - 17.6701\varsigma^{-1} + 6.78335 \right)
\tag{7}
$$

Substituting Equation (3) into Equation (4), the CSD of an RPLHGSM beam array in oceanic turbulence can be derived as:

$$
\begin{aligned}
W(\boldsymbol{\rho}_1, \boldsymbol{\rho}_2, z) = \frac{k^2}{4\pi^2 z^2} \exp\left[-\frac{ik}{2z}(\boldsymbol{\rho}_1^2 - \boldsymbol{\rho}_2^2) \right] \exp\left[-\frac{(\rho_{1x} - \rho_{2x})^2 + (\rho_{1y} - \rho_{2y})^2}{\Lambda_0^2} \right] \\
G_0 \sum_{h_1=1}^{N} \sum_{h_2=1}^{N} \frac{1}{H_{2m}(0)} \frac{1}{H_{2n}(0)} \exp\left[i(\varphi_{h_1} - \varphi_{h_2}) \right] \\
\sum_{l_x=0}^{m} \frac{(-1)^{l_x}(2m)!}{l_x!(2m-2l_x)!} \left(\frac{2}{\sqrt{2}\delta_{0x}} \right)^{2m-2l_x} \sum_{l_y=0}^{n} \frac{(-1)^{l_y}(2n)!}{l_y!(2n-2l_y)!} \left(\frac{2}{\sqrt{2}\delta_{0y}} \right)^{2n-2l_y} \\
W_x(\rho_x, z) W_y(\rho_y, z)
\end{aligned}
\tag{8}
$$

where

$$
\begin{aligned}
W_x(\rho_x, z) = \exp\left[-\frac{(r_{h_1x} - r_{h_2x})^2}{\Lambda_0^2} \right] \exp\left[-\frac{ik}{2z}(r_{h_1x}^2 - r_{h_2x}^2) \right] \exp\left[\frac{ik}{z}(\rho_{1x}r_{h_1x} - \rho_{2x}r_{h_2x}) \right] \\
\exp\left[-\frac{(\rho_{1x} - \rho_{2x})(r_{h_1x} - r_{h_2x})}{\Lambda_0^2} \right] \sum_{s_x=0}^{2m-2l_x} \frac{(2m-2l_x)!(-1)^{s_x}}{s_x!(2m-2l_x-s_x)!} \\
\sqrt{\frac{\pi}{a_x}} s_x! \left(\frac{1}{a_x} \right)^{s_x} \exp\left[\frac{1}{a_x}\left(-\frac{r_{h_1x} - r_{h_2x}}{\Lambda_0^2} - \frac{\rho_{1x} - \rho_{2x}}{2\Lambda_0^2} - \frac{ik}{2z}r_{h_1x} + \frac{ik}{2z}\rho_{1x} \right)^2 \right] \\
\sum_{t_x=0}^{\left[\frac{s_x}{2} \right]} \frac{1}{t_x!(s_x-2t_x)!} \left(\frac{a_x}{4} \right)^{t_x} \sum_{d_x=0}^{s_x-2t_x} \frac{(s_x-2t_x)!}{d_x!(s_x-2t_x-d_x)!} \\
\left(-\frac{r_{h_1x} - r_{h_2x}}{\Lambda_0^2} - \frac{\rho_{1x} - \rho_{2x}}{2\Lambda_0^2} - \frac{ik}{2z}r_{h_1x} + \frac{ik}{2z}\rho_{1x} \right)^{s_x-2t_x-d_x} \\
\left(\frac{1}{2\delta_{0x}^2} + \frac{1}{\Lambda_0^2} \right)^{d_x} \sqrt{\frac{\pi}{b_x}} \left(\frac{i}{2\sqrt{b_x}} \right)^{2m-2l_x-s_x+d_x} \exp\left(\frac{c_x^2}{b_x} \right) H_{2m-2l_x-s_x+d_x}\left(-\frac{ic_x}{\sqrt{b_x}} \right)
\end{aligned}
\tag{9}
$$

$$W_y(\rho_y, z) = \exp\left[-\frac{(r_{h_1y}-r_{h_2y})^2}{\Lambda_0^2}\right]\exp\left[-\frac{ik}{2z}\left(r_{h_1y}^2-r_{h_2y}^2\right)\right]\exp\left[\frac{ik}{z}\left(\rho_{1y}r_{h_1y}-\rho_{2y}r_{h_2y}\right)\right]$$

$$\exp\left[-\frac{(\rho_{1y}-\rho_{2y})(r_{h_1y}-r_{h_2y})}{\Lambda_0^2}\right]\sum_{s_y=0}^{2n-2l_y}\frac{(2n-2l_y)!(-1)^{s_y}}{s_y!(2n-2l_y-s_y)!}$$

$$\sqrt{\frac{\pi}{a_y}}s_y!\left(\frac{1}{a_y}\right)^{s_y}\exp\left[\frac{1}{a_y}\left(-\frac{r_{h_1y}-r_{h_2y}}{\Lambda_0^2}-\frac{\rho_{1y}-\rho_{2y}}{2\Lambda_0^2}-\frac{ik}{2z}r_{h_1y}+\frac{ik}{2z}\rho_{1y}\right)^2\right]$$

$$\sum_{t_y=0}^{[\frac{s_y}{2}]}\frac{1}{t_y!(s_y-2t_y)!}\left(\frac{a_y}{4}\right)^{t_y}\sum_{d_y=0}^{s_y-2t_y}\frac{(s_y-2t_y)!}{d_y!(s_y-2t_y-d_y)!}$$

$$\left(-\frac{r_{h_1y}-r_{h_2y}}{\Lambda_0^2}-\frac{\rho_{1y}-\rho_{2y}}{2\Lambda_0^2}-\frac{ik}{2z}r_{h_1y}+\frac{ik}{2z}\rho_{1y}\right)^{s_y-2t_y-d_y}$$

$$\left(\frac{1}{2\delta_{0y}^2}+\frac{1}{\Lambda_0^2}\right)^{d_y}\sqrt{\frac{\pi}{b_y}}\left(\frac{i}{2\sqrt{b_y}}\right)^{2n-2l_y-s_y+d_y}\exp\left(\frac{c_y^2}{b_y}\right)H_{2n-2l_y-s_y+d_y}\left(-\frac{ic_y}{\sqrt{b_y}}\right)$$

(10)

with

$$a_\beta = \frac{1}{4w_0^2}+\frac{1}{2\delta_{0\beta}^2}+\frac{1}{\Lambda_0^2}+\frac{ik}{2z}, (\beta = x, y) \tag{11}$$

$$b_\beta = \frac{1}{4w_0^2}+\frac{1}{2\delta_{0\beta}^2}+\frac{1}{\Lambda_0^2}-\frac{ik}{2z}-\frac{1}{a_\beta}\left(\frac{1}{2\delta_{0\beta}^2}+\frac{1}{\Lambda_0^2}\right)^2 \tag{12}$$

$$c_\beta = \frac{r_{h_1\beta}-r_{h_2\beta}}{\Lambda_0^2}+\frac{\rho_{1\beta}-\rho_{2\beta}}{2\Lambda_0^2}+\frac{ik}{2z}r_{h_2\beta}-\frac{ik}{2z}\rho_{2\beta}$$
$$+\frac{1}{a_\beta}\left(\frac{1}{2\delta_{0\beta}^2}+\frac{1}{\Lambda_0^2}\right)\left(-\frac{r_{h_1\beta}-r_{h_2\beta}}{\Lambda_0^2}-\frac{\rho_{1\beta}-\rho_{2\beta}}{2\Lambda_0^2}-\frac{ik}{2z}r_{h_1\beta}+\frac{ik}{2z}\rho_{1\beta}\right) \tag{13}$$

Based on the derived equations, the average intensity of an RPLHGSM beam array in oceanic turbulence is written as [9–19]:

$$I(\mathbf{r}, z) = W(\mathbf{r}, \mathbf{r}, z) \tag{14}$$

4. Numerical Results and Analysis

In this section, the average intensity characteristics of an RPLHGSM beam array transmitting in oceanic turbulence are analyzed. In the simulations, the parameters were chosen as $w_0 = 4$ mm, $\lambda = 532$ nm, $R = 6$ cm, $N = 4$, $m = n = 2$, $\varsigma = -2.5$, $\chi_T = 8 \times 10^{-8}$ K^2/s, $\varepsilon = 10^{-7}$ m^2 s^{-1} and $\eta = 1$ mm without other descriptions in the figures.
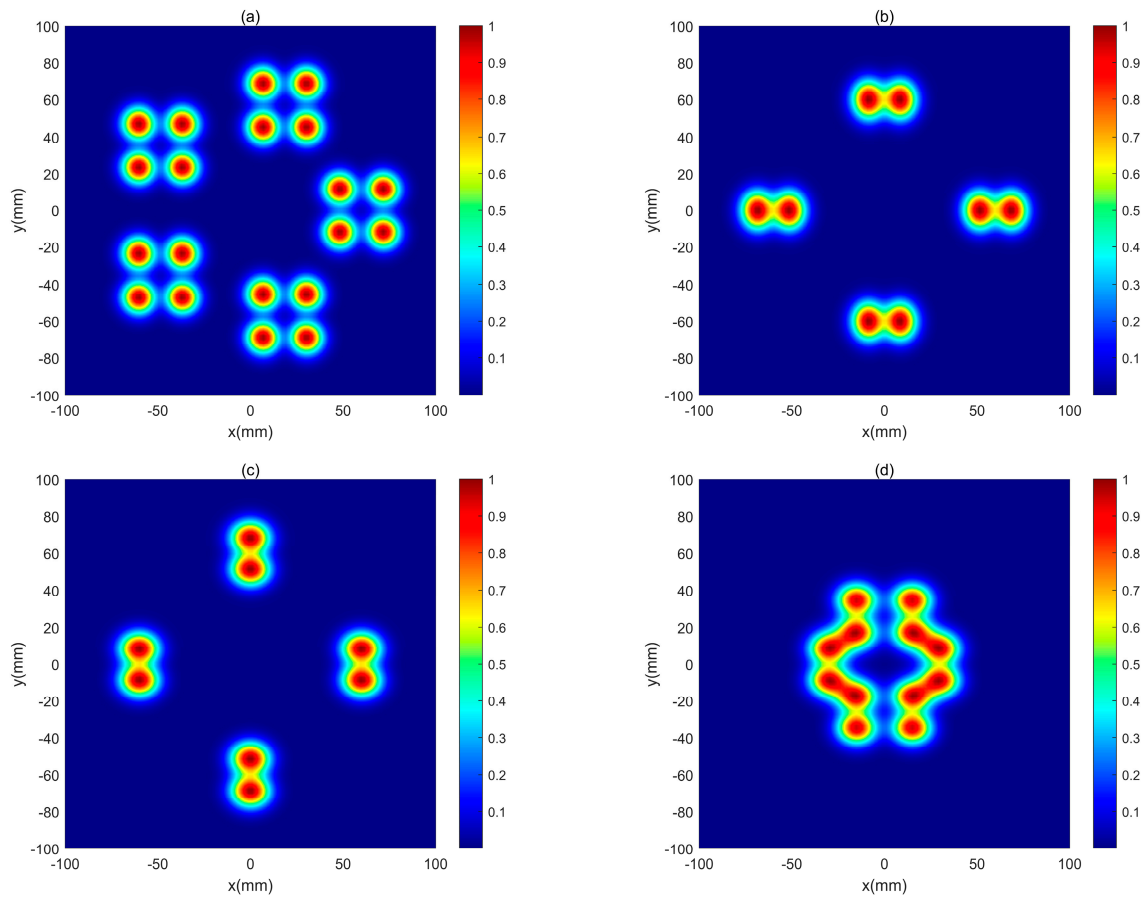
The intensity of an RPLHGSM beam array with $N = 4$ and $\delta_{0x} = \delta_{0y} = 3$ mm transmitting in free space is given in Figure 1. When the propagation distance is short, the intensity profile of an RPLHGSM beam array retains the four beam spots (Figure 1a). As the distance increases further, the sub-beam of an RPLHGSM beam array exhibits splitting properties, and the intensity distribution of an RPLHGSM beam array in free space becomes multiple beam spots, due to the influences of coherence $\delta_{0x} = \delta_{0y}$. The self-splitting phenomenon of the sub-beam is the same as the HGCSM beam [24]. Finally, the intensity profile of an RPLHGSM beam array shows multiple spots at $z = 200$ m (Figure 1d). Therefore, the intensity profile of an RPLHGSM beam array in free space is controlled by the initial beam number N and Hermite correlation function.
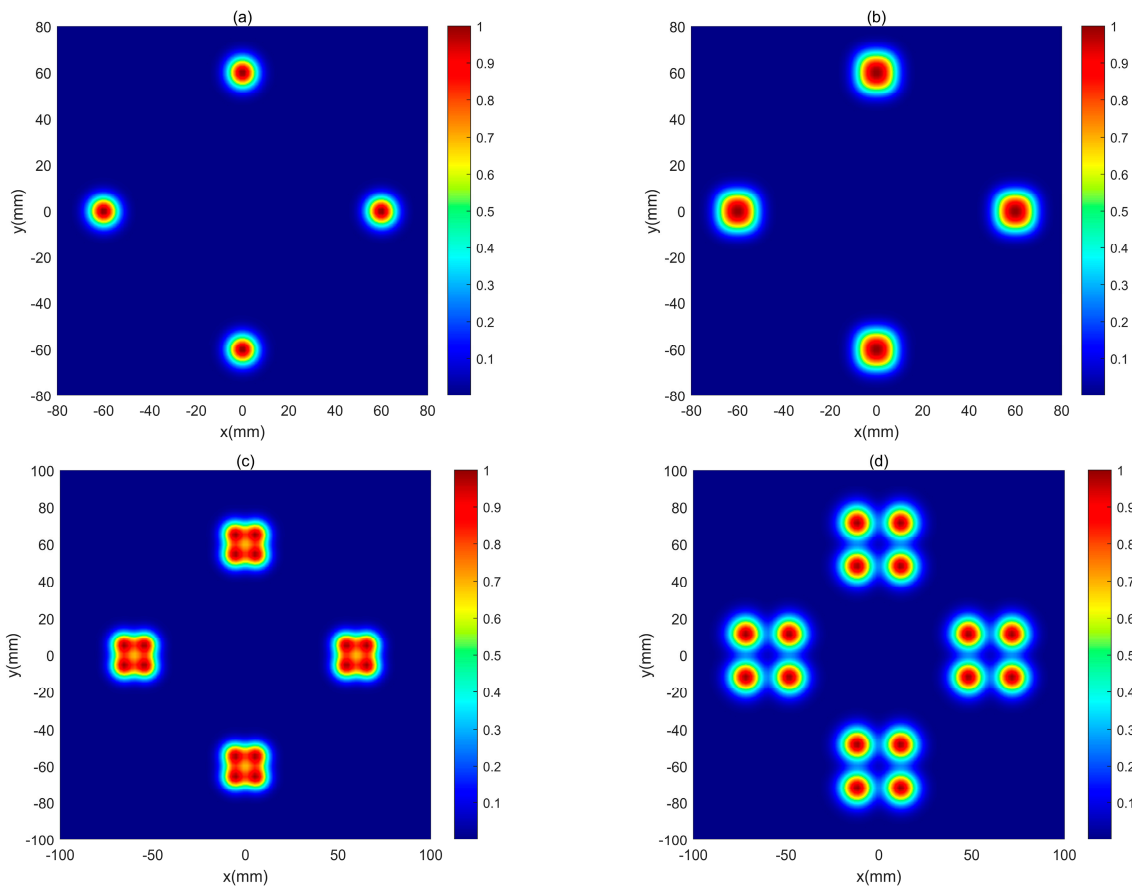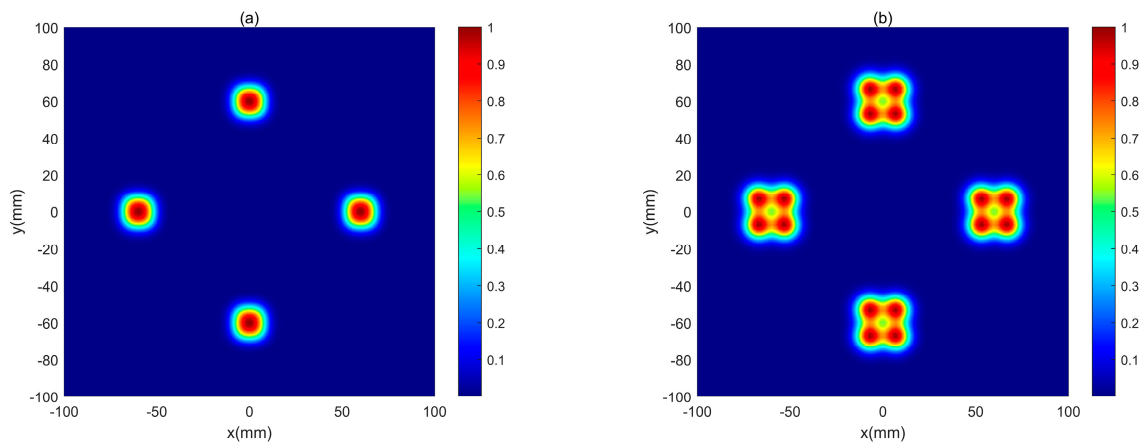
Figure 1. The intensity of an RPLHGSM beam array with $\delta_{0x} = \delta_{0y} = 3$ mm in free space. (**a**) $z = 30$ m, (**b**) $z = 60$ m, (**c**) $z = 100$ m, (**d**) $z = 200$ m.

The characteristics of an RPLHGSM beam array with $\delta_{0x} = \delta_{0y} = 3$ mm for the different initial beam parameters N, R, m and n transmitting in free space at $z = 200$ m are illustrated in Figure 2. From Figures 1d and 2a, it is found that the intensity profile of an RPLHGSM beam array has multiple spots, N affects the distribution of sub-beams, and the intensity pattern can be modulated by controlling the sub-beam number N. When the initial parameters m, n of sub-beams change, the intensity pattern of an RPLHGSM beam array has different intensity distributions. The intensity profile of the sub-beam is the same as the HGCSM beam with the same parameters in free space, however, the whole intensity pattern of an RPLHGSM beam array in free space is composed of different HGCSM beamlets (Figure 2a–c). When the radius R decreases, the multiple spots of the sub-beam of an RPLHGSM beam array overlap with the near sub-beams (Figure 2d), and the separate spot distributions are destroyed. Hence, we can adjust the intensity profiles of an RPLHGSM beam array in free space by modifying the initial beam parameters.

We considered the effects of an increase in the coherence length $\delta_{0x} = \delta_{0y}$. The intensity of an RPLHGSM beam array with larger $\delta_{0x} = \delta_{0y} = 5$ mm in free space is shown in Figure 3. It shows that the beamlet of an RPLHGSM beam array with larger $\delta_{0x} = \delta_{0y}$ in free space retains the single spot better at $z = 100$ m (Figure 3a), while the beam array with $\delta_{0x} = \delta_{0y} = 3$ mm splits into multiple spots (Figure 1c), an RPLHGSM beam array with smaller coherence length split fasters. Comparing Figure 3b with Figure 1d, an RPLHGSM beam array with larger $\delta_{0x} = \delta_{0y} = 5$ mm also split at $z = 200$ m, but the splitting phenomenon is not more apparent than for the beam array with $\delta_{0x} = \delta_{0y} = 3$ mm. Thus, the intensity distributions of an RPLHGSM beam array with smaller $\delta_{0x} = \delta_{0y}$ can retain the array profile better during propagation.
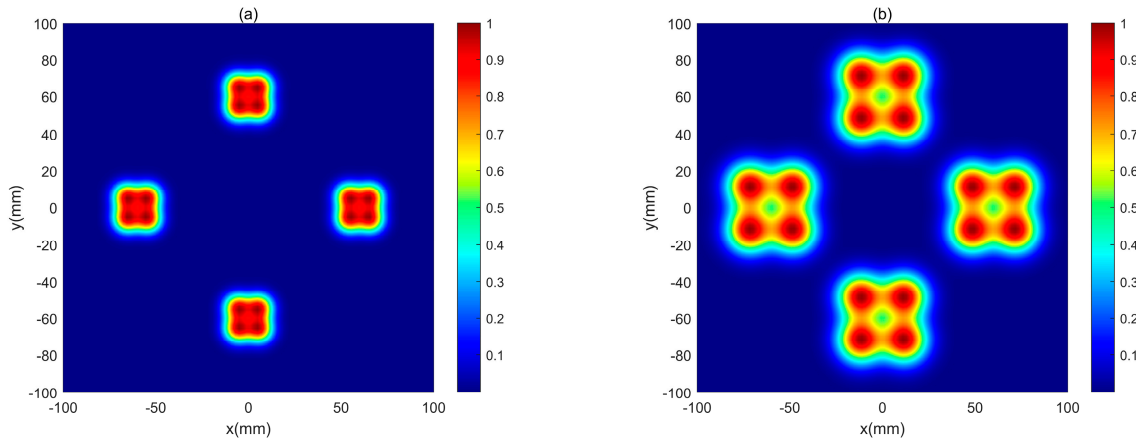
Figure 2. The intensity of an RPLHGSM beam array in free space at $z = 200$ m. (**a**) N = 5, R = 6 cm, $m = n = 2$, (**b**) $N = 4$, $R = 6$ cm, $m = 1$, $n = 0$, (**c**) N = 4, R = 6 cm, m = 0, n = 1, (**d**) $N = 4$, $R = 3$ cm, $m = 0$, $n = 1$.
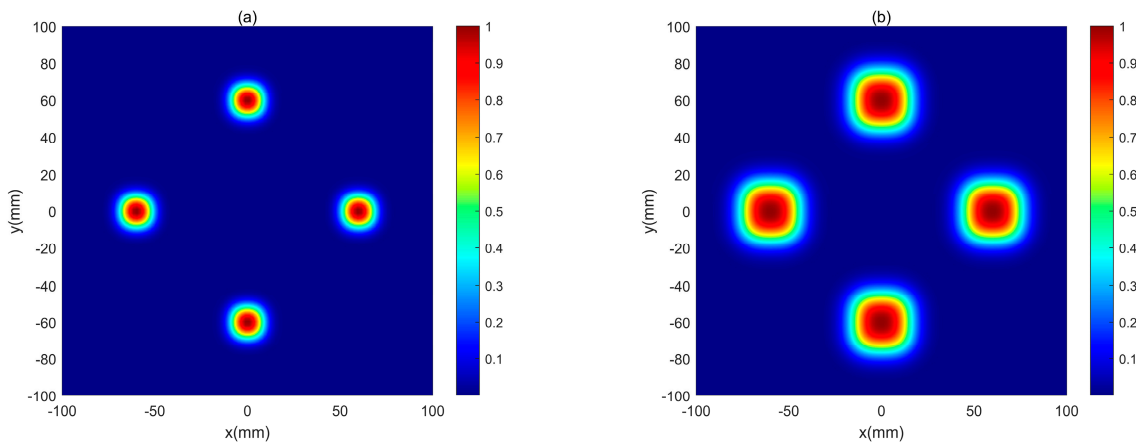
Figure 3. The intensity of an RPLHGSM beam array with $\delta_{0x} = \delta_{0y} = 5$ mm in free space. (**a**) z = 100 m , (**b**) $z = 200$ m.

Figures 4 and 5 show an RPLHGSM beam array with different $\delta_{0x} = \delta_{0y}$ propagating in oceanic turbulence. In Figure 4, the sub-beam of an RPLHGSM beam array with $\delta_{0x} = \delta_{0y} = 3$ mm in oceanic turbulence has combining properties (Figure 4b), while the same beam array in free space has separate spot profiles (Figure 1d). when $\delta_{0x} = \delta_{0y}$ increases, the sub-beam of an RPLHGSM beam array with $\delta_{0x} = \delta_{0y} = 5$ mm in oceanic turbulence becomes a spot, and this beam array in free space can retain multiple spot distribution (Figure 3b). Comparing Figures 3–5, the beam array with smaller $\delta_{0x} = \delta_{0y}$ better re-

tained its splitting properties during propagation on oceanic turbulence (Figures 4b and 5b). The combining properties of an RPLHGSM beam array can be seen in this example of beam array propagation in oceanic turbulence. (Figures 3b and 5b). Thus, the combining phenomenon of an RPLHGSM beam array in oceanic turbulence is affected by oceanic turbulence and coherence length, and a beam array with low coherence length retains its splitting properties better during propagation in oceanic turbulence.
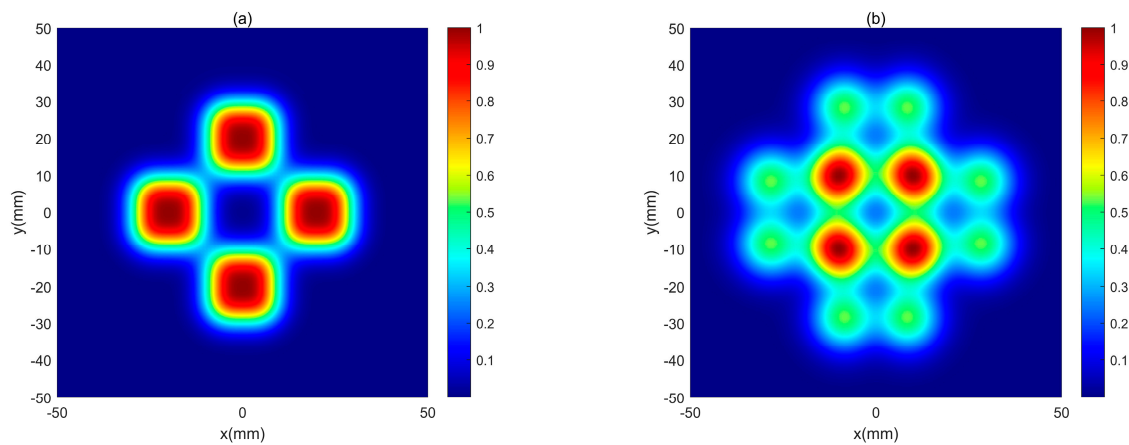

Figure 4. The intensity of an RPLHGSM beam array with $\delta_{0x} = \delta_{0y} = 3$ mm in oceanic turbulence. (**a**) $z = 100$ m, (**b**) $z = 200$ m.
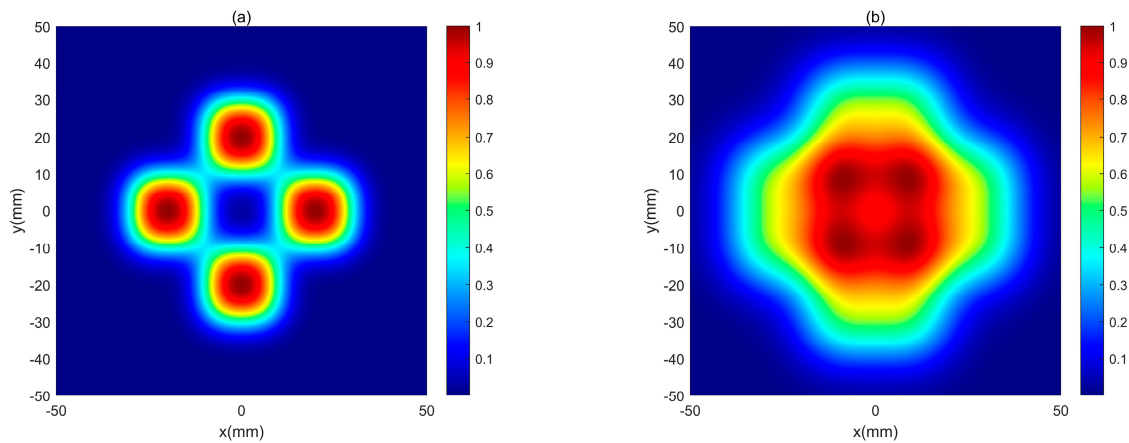

Figure 5. The intensity of an RPLHGSM beam array with $\delta_{0x} = \delta_{0y} = 5$ mm in oceanic turbulence. (**a**) $z = 100$ m, (**b**) $z = 200$ m.

When the radius R decreases, the intensity profiles of an RPLHGSM beam array with $N = 4$ and $R = 2$ cm transmitting through free space and oceanic turbulence are given in Figures 6 and 7. At $z = 100$ m, the intensity profile of sub-beam of an RPLHGSM beam array remains a spot profile. The sub-beam of this beam array splits at $z = 200$ m (Figure 6b), but the sub-beams of an RPLHGSM beam array in free space overlap with the surrounding sub-beams (Figure 6b) due to the reduction of R. While the same beam array in oceanic turbulence can evolve into one beam spot at $z = 200$ m, the combining properties of this beam array in oceanic turbulence are affected by radius R (Figures 5b and 7b). Therefore, the intensity profile of an RPLHGSM beam array in free space and oceanic turbulence can be modulated by controlling the parameter R and oceanic turbulence.

Figure 6. The intensity of an RPLHGSM beam array in free space. (**a**) $z = 100$ m, (**b**) $z = 200$ m.

Figure 7. The intensity of an RPLHGSM beam array in oceanic turbulence. (**a**) $z = 100$ m, (**b**) $z = 200$ m.

5. Conclusions

A new type of beam array, named RPLHGSM beam array, composed of N HGCSM sub-beams with radial distribution is proposed. The CSD of this beam array in oceanic turbulence was derived, and the influences of initial beam parameters and oceanic turbulence on evolution characteristics of this beam array are numerically discussed. The beamlets of an RPLHGSM beam array retain self-splitting properties in free space, the RPLHGSM beam array in free space can attain multiple spot distribution during propagation, and an RPLHGSM beam array with low coherence retains splitting properties better. The sub-beam of the same beam array transmitting in oceanic turbulence will overlap, and as R decreases, the profile of this beam array in oceanic turbulence becomes a beam spot. An RPLHGSM beam array with smaller coherence length in oceanic turbulence will retain its splitting properties better. The results confirm that an RPLHGSM beam array can have applications in underwater laser sensing and laser radar.

Institutional Review Board Statement: Not applicable.

Informed Consent Statement: Not applicable.

Data Availability Statement: Data is contained within the article.

Conflicts of Interest: The authors declare no conflict of interest.

References

1. Baykal, Y.; Ata, Y.; Gökçe, M.C. Underwater turbulence, its effects on optical wireless communication and imaging: A review. *Opt. Laser Technol.* **2022**, *156*, 108624. [CrossRef]
2. Wang, F.; Liu, X.L.; Cai, Y.J. Propagation of Partially Coherent Beam in Turbulent Atmosphere: A Review. *Prog. Electromagn. Res.* **2015**, *150*, 123–143. [CrossRef]
3. Klug, A.; Peters, C.; Forbes, A. Robust structured light in atmospheric turbulence. *Adv. Photonics* **2023**, *5*, 016006. [CrossRef]
4. Korotkova, O.; Farwell, N.; Shchepakina, E. Light scintillation in oceanic turbulence. *Waves Random Complex Media* **2012**, *22*, 260–266. [CrossRef]
5. Baykal, Y. Scintillation index in strong oceanic turbulence. *Opt. Commun.* **2016**, *375*, 15–18. [CrossRef]
6. Xu, G.; Lai, J. Scintillation index and BER performance for optical wave propagation in anisotropic underwater turbulence under the effect of eddy diffusivity ratio. *Appl. Opt.* **2020**, *59*, 2551–2558. [CrossRef]
7. Gercekcioglu, H. Bit error rate of focused Gaussian beams in weak oceanic turbulence. *J. Opt. Soc. Am. A* **2014**, *31*, 1963–1968. [CrossRef]
8. Zheng, Y.; Yang, D.Y.; Qin, S.Q.; Zhang, Y.X. Received Probability of Orbital-Angular-Momentum Modes Carried by Diffraction- and Attenuation- Resistant Beams in Weak Turbulent Oceans. *J. Mar. Sci. Eng.* **2020**, *8*, 701. [CrossRef]
9. Liu, X.; Zhou, G.; Shen, Y. Effect of oceanic turbulence with anisotropy on the propagation of multi-sinc Schell-model beams. *Results Phys.* **2022**, *36*, 105447. [CrossRef]
10. Liu, L.; Liu, Y.; Chang, H.; Huang, J.; Zhu, X.; Cai, Y.; Yu, J. Second-Order Statistics of Self-Splitting Structured Beams in Oceanic Turbulence. *Photonics* **2023**, *10*, 339. [CrossRef]
11. Xu, J.; Tang, M.M.; Zhao, D.M. Propagation of electromagnetic non-uniformly correlated beams in the oceanic turbulence. *Opt. Commun.* **2014**, *331*, 1–5. [CrossRef]
12. Wei, D.; Wang, K.; Xu, Y.; Du, Q.; Liu, F.; Liu, J.; Dong, Y.; Zhang, L.; Yu, J.; Cai, Y.; et al. Propagation of a Lorentz Non-Uniformly Correlated Beam in a Turbulent Ocean. *Photonics* **2023**, *10*, 49. [CrossRef]
13. Wang, X.; Wang, L.; Zhao, S. Research on Hypergeometric-Gaussian Vortex Beam Propagating under Oceanic Turbulence by Theoretical Derivation and Numerical Simulation. *J. Mar. Sci. Eng.* **2021**, *9*, 442. [CrossRef]
14. Liu, D.; Wang, G.; Yin, H.; Zhong, H.; Wang, Y. Propagation properties of a partially coherent anomalous hollow vortex beam in underwater oceanic turbulence. *Opt. Commun.* **2019**, *437*, 346–354. [CrossRef]
15. Ye, F.; Zhang, J.B.; Xie, J.T.; Deng, D.M. Propagation properties of the rotating elliptical chirped Gaussian vortex beam in the oceanic turbulence. *Opt. Commun.* **2018**, *426*, 456–462. [CrossRef]
16. Hu, Y.; Zhang, M.; Dou, J.; Zhao, J.; Li, B. Influences of salinity and temperature on propagation of radially polarized rotationally-symmetric power-exponent-phase vortex beams in oceanic turbulence. *Opt. Express* **2022**, *30*, 42772–42783. [CrossRef]
17. Zhan, H.; Peng, Y.; Chen, B.; Wang, L.; Wang, W.; Zhao, S. Diffractive deep neural network based adaptive optics scheme for vortex beam in oceanic turbulence. *Opt. Express* **2022**, *30*, 23305–23317. [CrossRef]
18. Liu, D.; Zhong, H.; Wang, G.; Yin, H.; Wang, Y. Radial phased-locked multi-Gaussian Schell-model beam array and its properties in oceanic turbulence. *Opt. Laser Technol.* **2020**, *124*, 106003. [CrossRef]
19. Tang, M.; Li, H. Statistical properties of twisted Gaussian Schell-model array beams in anisotropic ocean. *Optik* **2020**, *211*, 164612. [CrossRef]
20. Chen, Y.H.; Wang, F.; Cai, Y.J. Partially coherent light beam shaping via complex spatial coherence structure engineering. *Adv. Phys. X* **2022**, *7*, 2009742. [CrossRef]
21. Wang, H.; Peng, X.; Zhang, H.; Liu, L.; Chen, Y.; Wang, F.; Cai, Y. Experimental synthesis of partially coherent beam with controllable twist phase and measuring its orbital angular momentum. *Nanophotonics* **2022**, *11*, 689–696. [CrossRef]
22. Korotkova, O.; Sahin, S.; Shchepakina, E. Multi-Gaussian Schell-model beams. *J. Opt. Soc. Am. A* **2012**, *29*, 2159–2164. [CrossRef] [PubMed]
23. Zheng, S.; Huang, J.; Ji, X.; Cheng, K.; Wang, T. Rotating anisotropic Gaussian Schell-model array beams. *Opt. Commun.* **2021**, *484*, 126684. [CrossRef]
24. Chen, Y.H.; Liu, L.; Wang, F.; Zhao, C.L.; Cai, Y.J. Elliptical Laguerre-Gaussian correlated Schell-model beam. *Opt. Express* **2014**, *22*, 13975–13987. [CrossRef] [PubMed]
25. Chen, Y.H.; Gu, J.X.; Wang, F.; Cai, Y.J. Self-splitting properties of a Hermite-Gaussian correlated Schell-model beam. *Phys. Rev. A* **2015**, *91*, 013823. [CrossRef]
26. Song, Z.; Liu, Z.; Zhou, K.; Sun, Q.; Liu, S. Propagation characteristics of a non-uniformly Hermite–Gaussian correlated beam. *J. Opt.* **2016**, *18*, 015606. [CrossRef]
27. Liu, L.; Wang, H.; Liu, L.; Dong, Y.; Wang, F.; Hoenders, B.J.; Chen, Y.; Cai, Y.; Peng, X. Propagation Properties of a Twisted Hermite-Gaussian Correlated Schell-Model Beam in Free Space. *Front. Phys.* **2022**, *10*, 847649. [CrossRef]
28. Cai, Y.J.; Lin, Q.; Baykal, Y.; Eyyuboglu, H.T. Off-axis Gaussian Schell-model beam and partially coherent laser array beam in a turbulent atmosphere. *Opt. Commun.* **2007**, *278*, 157–167. [CrossRef]

29. Zhou, P.; Wang, X.L.; Ma, Y.X.; Ma, H.T.; Xu, X.J.; Liu, Z.J. Propagation of partially coherent partially phase-locked laser array in turbulent atmosphere. *Opt. Commun.* **2010**, *283*, 1071–1074. [CrossRef]

30. Yan, Y.; Wang, G.; Yin, Y.; Yin, H.; Wang, Y.; Liu, D. Radial phased-locked Laguerre-Gaussian correlated schell-model beam array. *Heliyon* **2022**, *8*, e11295. [CrossRef]

31. Lu, L.; Wang, Z.; Cai, Y. Propagation properties of phase-locked radially-polarized vector fields array in turbulent atmosphere. *Opt. Express* **2021**, *29*, 16833–16844. [CrossRef] [PubMed]

32. Ma, B.B.; Sun, C.; Lv, X.; Zhang, J.B.; Yang, X.B.; Wang, G.H.; Hong, W.Y.; Deng, D.M. Effect of turbulent atmosphere on the propagation of a radial phased-locked rotating elliptical Gaussian beam array. *J. Opt. Soc. Am. A* **2019**, *36*, 1690–1698. [CrossRef] [PubMed]

33. Jeffrey, A.; Dai, H.H. *Handbook of Mathematical Formulas and Integrals*, 4th ed.; Academic Press Inc.: Cambridge, MA, USA, 2008.

34. Zhang, Y.; Yang, K.; Li, P.; Wen, F.; Gu, Y.; Wu, Z. Generation of off-axis phased Gaussian optical array along arbitrary curvilinear arrangement. *Opt. Commun.* **2023**, *527*, 128967. [CrossRef]

35. Zhang, Y.; Hou, T.; Chang, Q.; Chang, H.; Long, J.; Ma, P.; Zhou, P. Propagation Properties of Gaussian Schell-Model Beam Array in the Jet Engine Exhaust Induced Turbulence. *IEEE Photonics J.* **2020**, *12*, 1–13. [CrossRef]

36. Zhao, J.; Wang, G.; Ma, X.; Zhong, H.; Yin, H.; Wang, Y.; Liu, D. Intensity and Coherence Characteristics of a Radial Phase-Locked Multi-Gaussian Schell-Model Vortex Beam Array in Atmospheric Turbulence. *Photonics* **2020**, *8*, 5. [CrossRef]

37. Nikishov, V.V.; Nikishov, V.I. Spectrum of Turbulent Fluctuations of the Sea-Water Refraction Index. *Int. J. Fluid Mech. Res.* **2000**, *27*, 82–98. [CrossRef]